Aerosol Science and Technology

ISSN: (Print) (Online) Journal homepage: https://www.tandfonline.com/loi/uast20

Using particle-resolved aerosol model simulations to guide the interpretations of cloud condensation nuclei experimental data

Patricia N. Razafindrambinina, Kotiba A. Malek, Anomitra De, Kanishk Gohil, Nicole Riemer & Akua A. Asa-Awuku

To cite this article: Patricia N. Razafindrambinina, Kotiba A. Malek, Anomitra De, Kanishk Gohil, Nicole Riemer & Akua A. Asa-Awuku (2023) Using particle-resolved aerosol model simulations to guide the interpretations of cloud condensation nuclei experimental data, Aerosol Science and Technology, 57:7, 608-618, DOI: 10.1080/02786826.2023.2202741

To link to this article: https://doi.org/10.1080/02786826.2023.2202741

AEROSOL SCIENCE AND TECHNOLOGY
2023, VOL. 57, NO. 7, 608–618
https://doi.org/10.1080/02786826.2023.2202741

Using particle-resolved aerosol model simulations to guide the interpretations of cloud condensation nuclei experimental data

Patricia N. Razafindrambinina[a], Kotiba A. Malek[b], Anomitra De[c], Kanishk Gohil[b], Nicole Riemer[d], and Akua A. Asa-Awuku[a,b]

[a]Department of Chemistry and Biochemistry, University of Maryland, College Park, Maryland, USA; [b]Department of Chemical and Biomolecular Engineering, University of Maryland, College Park, Maryland, USA; [c]Department of Chemical and Biomolecular Engineering, University of Illinois Urbana-Champaign, Urbana, Illinois, USA; [d]Department of Atmospheric Sciences, University of Illinois Urbana-Champaign, Urbana, Illinois, USA

ABSTRACT

Ambient aerosol particles can undergo dynamic mixing processes as they coagulate with particles from other air masses and emission sources. Therefore, aerosols exist in a spectrum, from externally mixed to internally mixed. The mixing state of aerosols can affect their ability to uptake water (hygroscopicity) and their cloud condensation nuclei (CCN) activity, modifying their contribution to the planet's total radiative budget. However, current water-uptake measurement methods may not be able to capture the complex mixing state. In this research, the dynamic mixing process was simulated by the particle-resolved aerosol model PartMC and also created by experiments in a laminar flow mixing tube. The mixing evolution of ammonium sulfate and sucrose binary mixtures were observed along with the changes in their water uptake properties expressed as the single hygroscopicity parameter, κ. The use of a mixing simulation in conjunction with experiments allow for better identification of the particle mixing state and the particle water uptake and show that no one kappa value can capture the complexity of mixing across the mixed particle size distribution. In other words, the PartMC simulations can be used as a guiding tool to interpret a system's mixing state based on its experimental droplet activation spectra. This work demonstrates the importance of the integration and use of mixing models to aid in mixing state determination and hygroscopicity measurements of mixed systems.

GRAPHICAL ABSTRACT

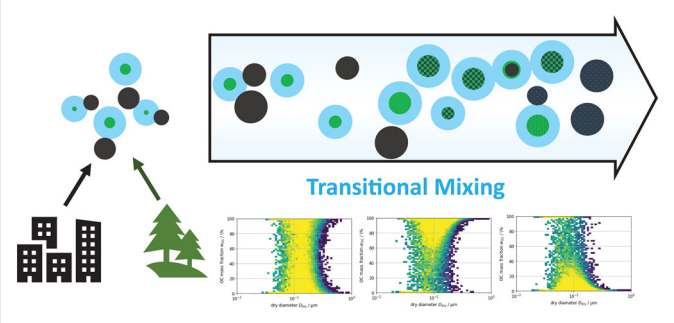

ARTICLE HISTORY
Received 14 August 2022
Accepted 28 March 2023

EDITOR
Kihong Park

Introduction

Organic and inorganic aerosol particles in the atmosphere come from natural sources such as volcanic eruptions, sea spray, and wildfires, as well as man-made sources like fossil fuel combustion and biomass burning. Aerosol particles often exist as a complex mixture and can undergo transport and aging processes in the atmosphere. The literature has defined the two extremes of aerosol mixing states as internally mixed and externally mixed, respectively (Winkler 1973). Internal mixing is present when all particles in the aerosol population have the same composition of chemical species. Each particle in an internally mixed aerosol can take on various

CONTACT Nicole Riemer nriemer@illinois.edu Department of Atmospheric Sciences, University of Illinois Urbana-Champaign, 1301 W Green St., Urbana, IL 61801-3028, USA; Akua Asa-Awuku asaawuku@umd.edu Department of Chemical and Biomolecular Engineering, University of Maryland at College Park, 4418 Stadium Drive, College Park, MD 20742-5031, USA.

Supplemental data for this article can be accessed online at https://doi.org/10.1080/02786826.2023.2202741.

morphologies which include homogenous, partially engulfed, and core-shell particles. In contrast, an externally mixed aerosol system consists of particles of pure chemical species with distinct compositions. An important concept, commonly assumed, is that for fully internal mixtures, all particles have the same hygroscopicity parameter κ. For fully external mixtures, several subpopulations exist that differ in their κ values, but within a subpopulation all particles have the same κ value.

In the atmosphere and under supersaturated conditions, aerosol particles can indirectly affect the planet's radiative forcing by acting as cloud condensation nuclei (CCN). In turn, clouds reflect solar radiation and may absorb longwave radiation emitted by the earth, which can lead to a cooling or heating impact on the atmosphere. It is known that particle composition, and therefore the mixing state of aerosols, play a key role in the system's CCN activity. However, the magnitude of the CCN influence on climate is still a topic of significant interest, as the spatial, temporal, and compositional complexity of aerosol particles lead to uncertainties in quantification of aerosol-cloud interactions and water uptake activity (Vu et al. 2019; Riemer et al. 2019).

Field studies have observed the mixing state of aerosols in the atmosphere. Cubison et al. (2008) demonstrated that knowledge of mixing state is an important parameter in predicting the activation of atmospheric aerosol particles at supersaturated conditions in the urban areas of Los Angeles, California (Cubison et al. 2008). More recently, Bondy et al. (2018) estimated the extent of internal versus external mixing of aerosol particles in the southeastern United States and reported that generally, externally mixed aerosols were more prevalent in the atmosphere (Bondy et al. 2018). Additionally, in the accumulation mode, internal mixing was more prominent during periods with high secondary organic aerosol (SOA) loadings, and external mixing dominated during high dust periods – further illustrating the complex nature of aerosol composition and mixing over time and space (Bondy et al. 2018). Observations of black carbon aerosols in the North China Plain by Wang et al. (2020) showed that the mixing state of aerosol particles is dynamic: freshly emitted black carbon aerosols are typically externally mixed and become more internally mixed over time (Wang et al. 2020).

The mixing state of aerosol particles, along with their sizes and compositions, has been shown to modify particle water uptake (Cubison et al. 2008; Hudson 2007; Dusek et al. 2006; Feingold 2003; Roberts et al. 2002). For example, Xu et al. (2020) measured the subsaturated water uptake of wintertime aerosol particles at Mace Head, Ireland, as a single hygroscopicity parameter (κ) using a humidified tandem differential mobility analyzer (HTDMA) and reported hygroscopicities between 0.3 and 0.5 for particles from 35 nm to 165 nm in diameter (Xu et al. 2020; Petters and Kreidenweis 2007). It was also emphasized that wintertime aerosol was observed to be largely externally mixed for both continental and marine air masses (Xu et al. 2020). In contrast, Kim et al. (2020) measured the hygroscopicity of urban aerosols in Seoul, Korea to have κ values between 0.15 to 0.3, lower than those reported by Xu et al. (2020) and Andreae and Rosenfeld (2008) (Kim et al. 2020; Xu et al. 2020; Andreae and Rosenfeld 2008). It was also reported that during their measurement period, externally mixed aerosols dominated the population (over 70%) in 100 nm and 150 nm particles. For small particles between 30 nm to 50 nm, internally mixed aerosols with a growth factor (GF) less than 1.1 constituted over 50% of the population (Kim et al. 2020). A separate study estimated that internally mixed aerosols in the central North China Plain to have $\kappa = 0.31$ and that this can change with time and age of the particles (Wang et al. 2020).

From the studies above, it can be inferred that the assumption of fully external or internal mixing can be a source of uncertainty in particle hygroscopicity predictions over time and space. Moreover, an externally mixed aerosol implies that subpopulations with different kappa values potentially exist. As such, there is a need for research into the effect of particle composition and mixing state on water-uptake under controlled conditions. Laboratory studies have demonstrated that the water uptake of inorganic salts such as ammonium sulfate may change in the presence of soluble organics, pointing toward the effect and importance of composition in overall particle hygroscopicity (Razafindrambinina et al. 2022; Lei et al. 2014). Lei et al. (2014) found that for internal mixtures of levoglucosan and ammonium sulfate, water uptake was continuous between 5% to 90% RH, suggesting that highly oxidized organics like levoglucosan may hold a key role in controlling the subsaturated water uptake properties of atmospheric particles (Lei et al. 2014). Cruz and Pandis (1998) measured the CCN activity for organic (glutaric acid) coated ammonium sulfate aerosol particles and found that the hygroscopic organic coating increased the CCN activation of ammonium sulfate particles and observations could be well predicted *via* Köhler theory (Cruz and

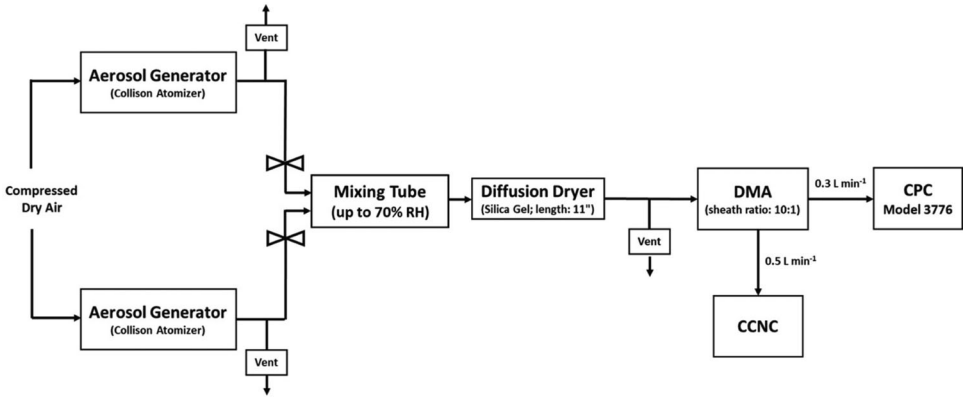

Figure 1. Schematic of the experimental setup for CCN measurement.

Pandis 1998). Work by Svenningsson et al. (2006) measured the subsaturated and supersaturated water uptake of several mixtures of ammonium sulfate, levoglucosan, succinic acid, and fulvic acid using a HTDMA and a cloud condensation nuclei spectrometer (Svenningsson et al. 2006). Mixed particle hygroscopicity for mixtures were accurately predicted by using the Zdanovskii-Stokes-Robinson (ZSR) model, assuming volume additivity and taking into account the limited solubility of succinic acid (Svenningsson et al. 2006).

Fewer studies have observed and quantified the dynamically evolving mixing state of aerosol particles under controlled laboratory conditions. In this manuscript, we refer to this evolution in aerosol composition as *transitional* mixing where the aerosol population is neither fully externally nor fully internally mixed. Vu et al. (2019) measured the cloud condensation nuclei activation of two-component organic and inorganic systems under internal, external, and transitional mixing conditions with the use of a laminar flow mixing tube. Separate aerosols streams of ammonium sulfate and succinic acid were generated and allowed to mix, and it was shown that mixing dry, non-hygroscopic particles with hygroscopic aerosol particles in a laminar flow mixing tube allowed for the observation of the dynamic mixing state transition from external to internally mixed (Vu et al. 2019).

It is challenging to discern the effects of mixing state from atmospheric aerosol of unknown sources. The work presented here minimizes the influences of unknown parameters and focuses on two individually well-described inorganic and organic aerosol systems. We utilized a binary system of ammonium sulfate and sucrose to demonstrate the evolution of hygroscopicity of the population as the two particle types interact due to coagulation in the flow tube. Ammonium sulfate is a prevalent inorganic aerosol species formed in the atmosphere from precursors sulfuric acid and ammonia (Behera et al. 2013; Aneja et al. 2008). Sucrose is an organic compound that exists in the ambient aerosol and is used as a tracer aerosol particle for biomass burning (Marynowski and Simoneit 2022).

The stochastic particle-resolved aerosol model PartMC (Riemer et al. 2009) predicted the evolution of the system and was used to help interpret the experimental findings of particle water uptake considering the evolving mixing states. PartMC has been used in prior studies to simulate fresh soot aerosol as it ages and mixes with other types of aerosols such as mineral dust and inorganic particles (Tian et al. 2014; Zaveri et al. 2010; Riemer et al. 2009). The model has also been applied to simulate aerosol evolution in laboratory settings (Shou et al. 2019; Tian et al. 2017).

Materials and methods

Experimental setup

Dilute solutions (0.3 g/L) of ammonium sulfate (98%, Millipore) and sucrose (99% Fisher Chemical) were each prepared by dissolving the solids in ultrapure water (Milli-Q 7003) and each solution was atomized into a polydisperse aerosol stream by a constant output atomizer (TSI 3076) according to the setup in Figure 1.

Polydisperse aerosol was generated at a flow rate of 1.1 ± 0.1 L min^{-1} and directed into a 0.1 m^3 laminar flow mixing tube. Vents downstream of each atomizer were incorporated into the setup to prevent a build-up of pressure in the system. Details on the mixing tube design is presented in published literature (Vu et al. 2019). In this experiment, valves were added upstream of the mixing tube to control the introduction of aerosol particles into the tube. Initial conditions for the experiments are presented in Table 1. It should be noted that the RH is not constant within the tube over the course of the experiment in this

Table 1. Initial experimental conditions in the mixing tube.

Chemical	Solubility @ 298 K (g/L)	Molecular Weight (g/mol)	Density (g/mL)	κ_{theory}	Supersaturation (%)	Volume Fraction	Center of Distribution (nm)
Sucrose	2040[a]	342.3	1.59[a]	0.08	0.80 ± 0.04	0.5	131
Ammonium Sulfate	764[b]	132.1	1.77[b]	0.6		0.5	117.8

study. It is possible that the relative humidity in the mixing tube may facilitate or accelerate the dynamic mixing state toward a fully internally mixed system. A previous paper has shown this to be the case for AS + succinic acid (Vu et al. 2019) and Ye et al. 2016 have shown that the presence of water may promote mixing aerosol. Additional simulations were conducted to explore the effect of varying initial input sizes (see the online supplemental material (SI), Figure S1). No visible condensation was observed in the mixing flow tube. Furthermore, particles are subsequently dried before particle size and CCN activity measurement.

In this work, two mixing directions were studied. The forward mixing experiment is when ammonium sulfate was introduced into a system of pure sucrose, and the reverse mixing experiment is when sucrose was added into a system of pure ammonium sulfate in the mixing tube. Mixing state experiments consisted of three distinct phases. For Phase 1 of the forward mixing experiment, only the organic aerosol was present in the mixing tube. At the beginning of Phase 2, ammonium sulfate was introduced into the mixing tube. Both ammonium sulfate and sucrose aerosol particles were continuously injected into the mixing tube during this phase. In Phase 3, the sucrose supply was terminated, which allowed ammonium sulfate to become the only species present in the tube. For the reverse reaction, Phase 1 started with pure ammonium sulfate, and Phase 3 ended with pure sucrose. Each phase was considered complete when the residence time of the mixing tube (2 h) had elapsed.

Water-uptake measurements under supersaturated conditions

Prior to water uptake measurements, particles were sampled from the mixing tube at 0.8 L min^{-1} through a diffusion dryer to create a dry, polydisperse aerosol stream. Dry polydisperse aerosol particles were subsequently size selected by an electrostatic classifier with a differential mobility analyzer (DMA; TSI 3081) which scanned electrical mobility diameters between 14 nm to 600 nm. Downstream of the DMA, aerosols were split between the condensation particle counter (CPC; TSI 3776) with a sample flow of 0.3 L min^{-1} and the cloud condensation nuclei counter (CCNC; DMT CCN-100) with a sample flow of 0.5 L min^{-1}. The CCNC provided the number of activated particles at a given supersaturation (CCN), and the CPC provided the size distribution and total number of all particles (CN). The Python-based CCN analysis tool (PyCAT) software was used to align the timeseries from the CPC and CCNC and estimate the fraction of activated particles. This software is based on the scanning mobility CCN analysis program by Moore, Nenes, and Medina (2010), with additional features that allow the fitting of more than one activation curve per scan (Gohil and Asa-Awuku 2022; Moore, Nenes, and Medina 2010). A sigmoid curve was then fit to the data to retrieve the mixed particles' activation diameter (D_{p50}), which is the dry particle diameter at which half of the total population activates into droplets at a given supersaturation, from the size resolved particle count from the SMPS and droplet count from the CCNC (Moore, Nenes, and Medina 2010). In this CCN analysis, it is assumed that the composition of the activation diameter can be applied across the entire size distribution. The Scanning Mobility CCN Analysis setup has been shown to produce approximately 120 data points during a single 135 s scan. Notably, previous studies have done similar analyses by keeping aerosol diameter constant and then modifying the supersaturation. However, the resolution of data from the CCN activation spectrum at a constant diameter produces fewer data points unless one uses a Scanning Flow CCN Analysis set-up (Moore and Nenes 2009).

Hygroscopicity analysis

Water uptake of a single-component system (or a fully internally-mixed system) can be represented by the single hygroscopicity parameter (κ) (e.g., Petters and Kreidenweis 2007, Lambe et al. 2011, Kreidenweis and Asa-Awuku 2014, Zhao et al. 2015, Fofie, Donahue, and Asa-Awuku 2018, Dawson et al. 2020, Peng et al. 2021, Peng et al. 2021; Dawson et al. 2020; Fofie, Donahue, and Asa-Awuku 2018; Zhao et al. 2015; Kreidenweis and Asa-Awuku 2014; Lambe et al. 2011; Petters and Kreidenweis 2007). The parameter κ is composition-dependent, which allows for hygroscopicity comparisons across instruments and relative humidities (Petters and Kreidenweis 2007, 2008, 2013). For supersaturated water uptake measurements,

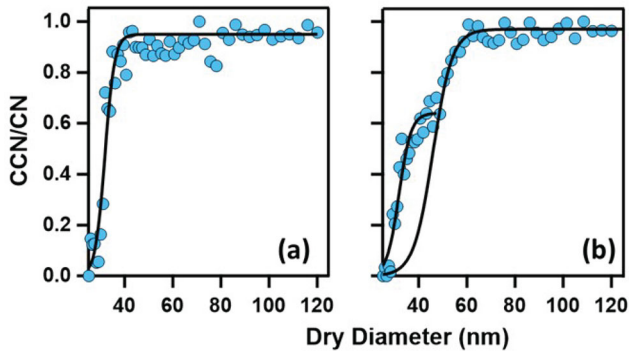

Figure 2. Pure ammonium sulfate (a) and externally (b) mixed ammonium sulfate-sucrose aerosol activation curves. Measured data is presented as blue circles, sigmoid fits used to estimate Dp50 is shown as black lines. Note that in (b), two sigmoid fits are present.

κ can be calculated from the estimated D_{p50} using Equation (1), based on κ-Köhler theory (Petters and Kreidenweis 2007; Lambe et al. 2011; Zhao et al. 2015; Peng et al. 2021; Fofie, Donahue, and Asa-Awuku 2018; Kreidenweis and Asa-Awuku 2014; Dawson et al. 2020).

$$\kappa = \frac{4\left(\frac{4\sigma_{s/a}M_w}{RT\rho_w}\right)^3}{27D_{p50}^3 S} \quad (1)$$

The variables $\sigma_{s/a}$, M_w, ρ_w are the surface tension, molecular weight, and density of water, R and T are the universal gas constant and temperature, respectively. D_{p50} is the critical activation diameter and S is the instrument supersaturation.

For internally mixed aerosols, κ can be estimated based on the Zdanovskii-Stokes-Robinson (ZSR) model (Stokes and Robinson 1966; Petters and Kreidenweis 2007). The ZSR model estimates the κ-value of a system based on the volume fraction (ϵ) of each solute, i, assuming that the solutes take up water independently, and do not interact with each other (Equation (2))

$$\kappa = \sum_i \epsilon_i \kappa_i \quad (2)$$

Equation (2) assumes that all particles are fully soluble, and the assumption has been demonstrated to hold for mixed ammonium sulfate-sucrose systems as both are fully soluble under experimental conditions. (Razafindrambinina et al. 2022)

In contrast, for fully externally mixed aerosols, each solute retains the κ of the pure compound. In other words, a fully external mixture of N aerosol species will have N D_{p50} and κ-values (Vu et al. 2019). Figure 2 illustrates how external mixtures can be distinguished from internal mixtures through the particle activation curves, and this concept has been well described in the literature (Vu et al. 2019; Lance et al. 2013).

PartMC simulations

PartMC is a stochastic, particle-resolved aerosol box model that resolves the composition of many individual aerosol particles within a well-mixed volume of air. The numerical methods used in PartMC have been described in detail in previous literature (Riemer et al. 2009; DeVille, Riemer, and West 2011, 2019; Curtis et al. 2016). To summarize, the particle-resolved approach uses a large number of discrete computational particles (10^4 to 10^6) to represent the particle population of interest. Each particle is represented by a "composition vector", which stores the mass of each constituent species within each particle and evolves over the course of a simulation according to various chemical or physical processes. For our study, the relevant process is Brownian coagulation, which is simulated with a stochastic Monte Carlo approach by generating a realization of a Poisson process. The "weighted flow algorithm" improves the model efficiency and reduces ensemble variance (DeVille, Riemer, and West 2011, 2019). The code is open-source under the GNU General Public License (GPL) version 2 and can be downloaded at http://github.com/compdyn/partmc/. We used version 2.6.0 for this work.

To illustrate the formation of mixed particles in the mixing tube, we set up a PartMC box model simulation using size distribution parameters informed by the experiment. We simulated the two cases described above ("forward" and "reverse" experiment). We assumed that the mixing tube experiments can be approximated by a plug-flow-reactor set up, starting with one size distribution of ammonium sulfate or sucrose (Phase 1 and Phase 3), or two externally mixed size distributions of ammonium sulfate and sucrose (Phase 2). This assumes that turbulent mixing along the flow direction can be neglected. The initial particle size distributions, informed by the experiments, are listed in Table 2. It should be noted that a dry aerosol system is assumed in the model and thus simulations are likely a lower estimate of coagulations rates. Additional simulations were conducted at varying initial input sizes; coagulation rates did vary however the overall conclusions regarding mixing state are similar (see the SI, Figure S1).

The PartMC simulations predicted the evolution of the aerosol populations during the residence time in the mixing tube, given by the volume of the tube divided by the flow rate (about 70 to 80 min for the experimental conditions in this paper), from the time

of injection into the mixing tube to the time of sampling. During this time, the particles coagulated with each other, decreasing the total number concentration and, in the case of the Phase-2 simulations, forming a subpopulation of mixed particles. The number of computational particles for these simulations was 100,000. For simplicity we neglected wall losses.

Table 2. Initial particle size distribution for PartMC simulations. AS stands for ammonium sulfate.

Forward direction: Sucrose to AS			
Component	N m^{-3}	D_{pg} / m	σ
Phase 1			
Sucrose	8.18×10^{11}	4.56×10^{-8}	1.73
Phase 2			
Sucrose	3.72×10^{11}	4.56×10^{-8}	1.73
AS	7.09×10^{11}	4.38×10^{-8}	1.81
Phase 3			
AS	1.30×10^{12}	4.38×10^{-8}	1.81
Reverse Direction: AS to Sucrose			
Component	**N m^{-3}**	**D_{pg} / m**	σ
Phase 1			
AS	9.31×10^{11}	4.54×10^{-8}	1.8
Phase 2			
AS	$4.10E \times 10^{11}$	4.54×10^{-8}	1.8
Sucrose	$7.39E \times 10^{11}$	6.57×10^{-8}	1.93
Phase 3			
Sucrose	1.32×10^{12}	6.57×10^{-8}	1.93

Results and discussion

The particle growth measured by the CCNC results in activation curves as shown in Figure 3a. For Phase 1 of the forward mixing experiment, only sucrose is present in the mixing tube, and a sample activation curve (sampled 30 min after sucrose injection) is presented in Figure 3a. The measured activation curve of sucrose was fit to a single sigmoid function using the PyCat algorithm ($\kappa = 0.08$). Figure 3b shows the two-dimensional number distribution $n(D_{dry},\kappa)$ distribution of the system as predicted by PartMC after 80 min of simulation. Since only sucrose is present, all particles had the same κ value, equal to $\kappa_{sucrose}$. The orange, black and green lines in Figure 3b indicate lines of constant critical supersaturation. The particles to the right of these lines have critical supersaturation lower than the respective threshold value, and the particles to the left of the lines have critical supersaturations higher than the threshold value. Activation curves can also be constructed using PartMC output, and for 0.86% supersaturation, the predicted activation curve agreed well with the experimental data obtained at the same supersaturation. During Phase 1, since only a single component

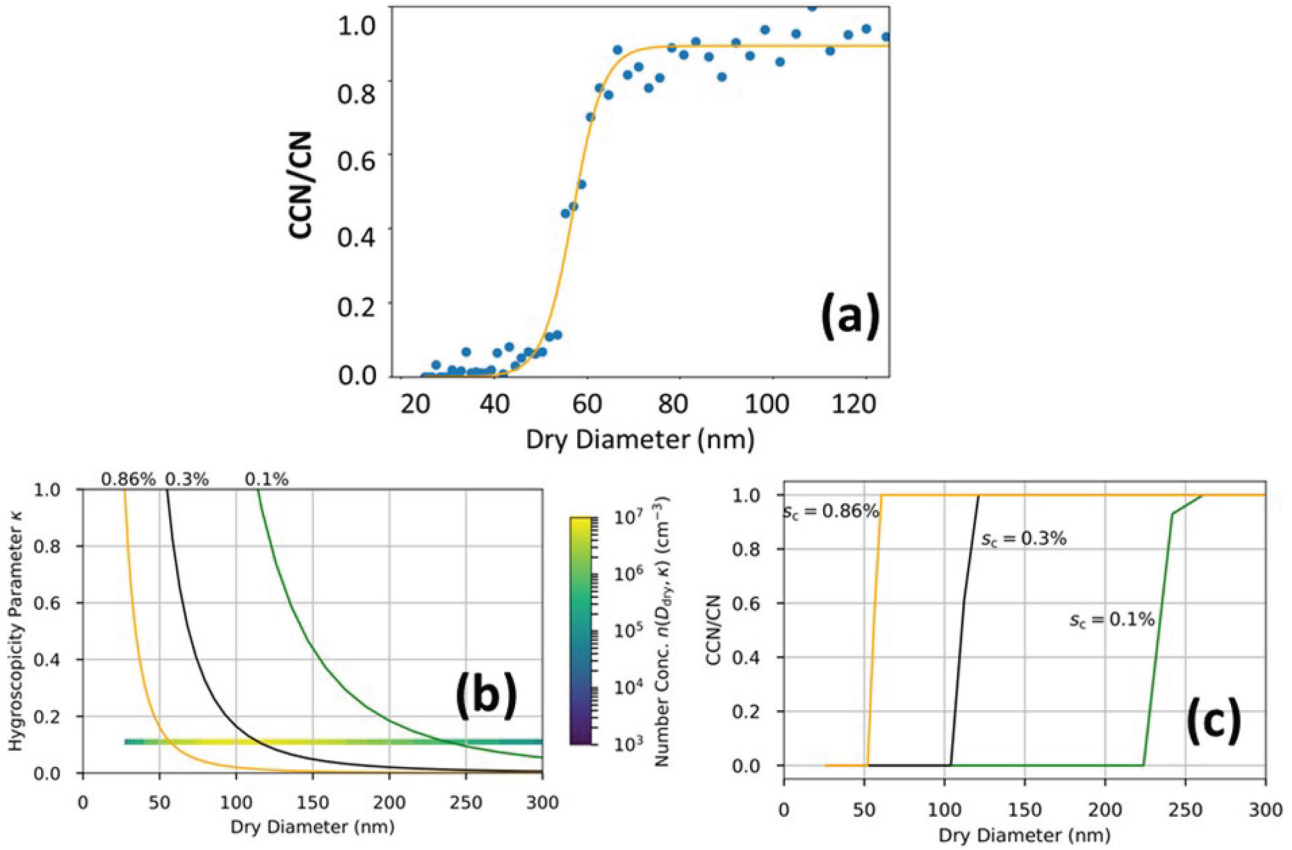

Figure 3. Experimental and simulated data for Phase 1 of the forward mixing (sucrose to ammonium sulfate) experiment: (a) Activation curve of experimental data points (solid symbols), and the single sigmoid fit generated by PyCat (solid orange line), (b) PartMC simulated $n(D_{dry},\kappa)$ distribution, and (c) PartMC-generated activation curves.

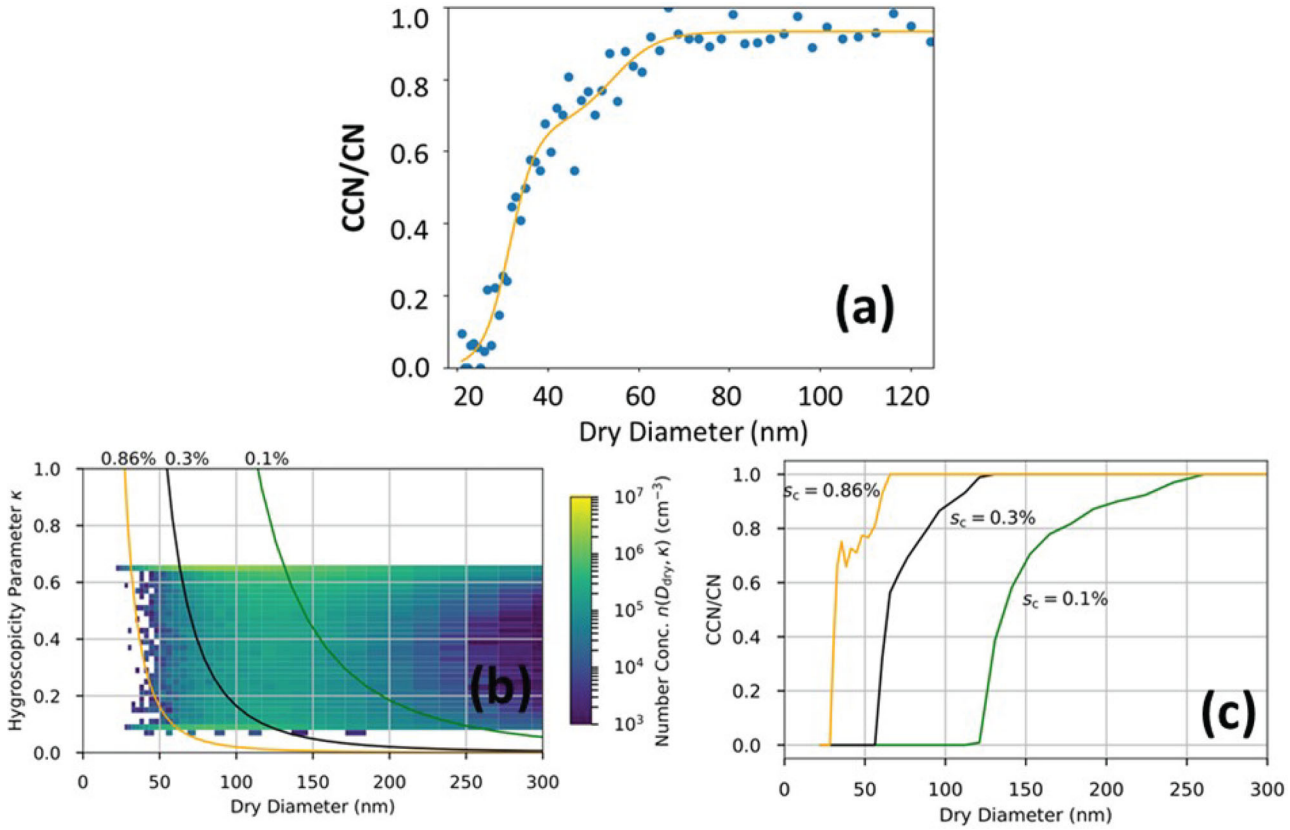

Figure 4. Experimental and simulated data for phase two of the forward mixing experiment which includes: (a) Activation curve of experimental data points (solid symbols), and the double-sigmoid fit generated by PyCat (solid orange line), (b) PartMC simulated $n(D_{dry},\kappa)$ distribution, and (c) PartMC-generated activation curves. Solid orange, black, and green lines represent 0.86%, 0.3%, and 0.1% supersaturation.

was present in the tube (sucrose), the activation curve predicted by PartMC was a step function, as expected. In comparison, the experimental activation curve was more of a smooth sigmoid function due to uncertainties in particle number counting.

Figure 4a shows a sample activation curve (sampled 75 min after ammonium sulfate injection) from Phase 2 of the same forward mixing experiment. The activation curve displays two distinct plateaus at CCN/CN $\approx$ 0.5 and at CCN/CN = $\sim$1.0, indicating the presence of a system with more than one aerosol type, similar to what was shown in Figure 2b. The PyCat algorithm fits a sigmoid curve over each distinct plateau over the experimental activation curves and retrieved two distinct κ-values: 0.2 and 0.6. The interpretation of this result is that at the supersaturation of 0.86%, the aerosol population appears externally mixed, consisting of two components, with κ of 0.2 and 0.6, respectively. $\kappa = 0.6$ is indicative of ammonium sulfate, and $\kappa = 0.2$, which is higher than the κ-value of sucrose ($\kappa_{sucrose} = 0.08$), may be indicative of a partial internal mixture that has begun to form. The corresponding simulated activation curve is depicted as orange line in Figure 4c. The simulated activation curve for the supersaturation of 0.86% also shows the two distinct plateaus. However, the two experimentally retrieved κ-values at one particular supersaturation do not capture the complexity of the full hygroscopicity distribution in a system of coagulating particles which forms particles that cover a continuous range of κ. This is illustrated in Figure 4b where we see the simulated $n(D_{dry},\kappa)$ distribution after 75 min of simulation. Due to the process of coagulating sucrose and ammonium sulfate particles, the space between $\kappa = 0.65$ and $\kappa = 0.08$ filled out, resulting in a fairly continuous $n(D_{dry},\kappa)$ distribution. An exception is the diameter range below 50 nm, which coincides with the size range that the line $s_c = 0.86\%$ intersects. Although some particles in this size range consist of sucrose/ammonium sulfate mixtures, most of the particles are still either ammonium sulfate or pure sucrose. The reason for this is the coagulation dynamics. Coagulation events between large and small particles are more likely and therefore producing mixed particles of diameters smaller than 50 nm is not favored given the initial size distributions used here. As a result, the activation curve at this supersaturation resembles that of an

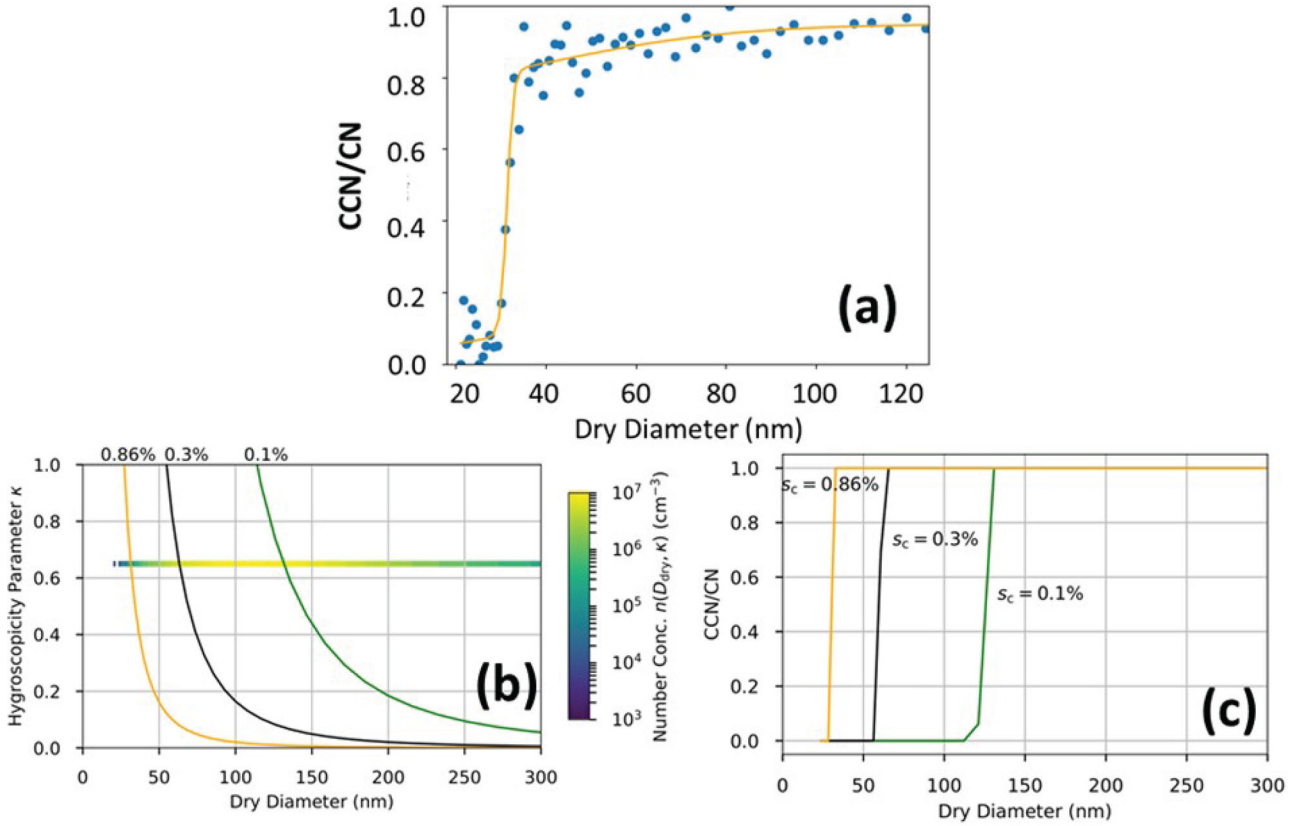

Figure 5. Experimental and simulated data for phase three of the forward mixing experiment which includes: (a) Activation curve of experimental data points (solid symbols), and the single sigmoid fit generated by PyCat (solid orange line), (b) PartMC simulated $n(D_{dry},\kappa)$ distribution of the system, and (c) PartMC-generated activation curves. Solid orange, black, and green lines represent 0.86%, 0.3%, and 0.1% supersaturation conditions.

external mixture as we have seen in Figure 4a and c, even though the population at larger sizes is not externally mixed. For comparison, Figure 4c also includes the activation curves for 0.3% and 0.1% supersaturation based on the PartMC simulation results. In contrast to the activation curve for 0.86%, they do not display a secondary plateau but increase indeed smoothly across the diameter range. This behavior can be understood by comparing to Figure 4b. The lines of constant critical supersaturation for 0.3% and 0.1% intersect the $n(D_{dry},\kappa)$ distribution at diameter ranges where a continuum of κ values exist. Therefore, as the diameter increases, the CCN/CN fraction smoothly increases.

Although PyCat sigmoid fits and retrieved κ-values for 0.86% are sound, the current experimental setup is unable to probe the complete $n(D_{dry},\kappa)$ distribution as simulated by PartMC. To do this, activation curves at lower supersaturations would need to be measured, or smaller particles should be used.

Phase 3 began when the injection of the aerosol species that was introduced first during Phase 1 was ceased. In the case of the forward mixing experiments, only ammonium sulfate was being injected into the mixing tube. Particle activation at two hours into phase 3 of the forward mixing experiment is shown as the activation curve in Figure 5a. The double activation curve seen in Phase 2 (Figure 4a) evolved into a single activation as sucrose in the mixing tube had been removed, and ammonium sulfate became the sole species in the system. This experimental result matched the simulated activation curves by PartMC (Figure 5b and c).

Results show that PyCat analysis and PartMC simulations are comparable for single component systems, as only a single κ-value is retrieved. However, the stochastic process of coagulation leads to a population of particles with a continuous distribution of hygroscopicities between the minimum κ value of pure sucrose particles and the maximum κ value of pure ammonium sulfate particles. Although the various hygroscopicity subpopulation is shown in the PartMC simulations, not all discrete κ-values were able to be identified in the experimental data. Although the size-resolved measurement method used in the experiment currently provides over one data point per second, only two sigmoids were able to be distinguished per scan. Additionally, the inflection points and plateau of each sigmoid must be distinct enough from each other

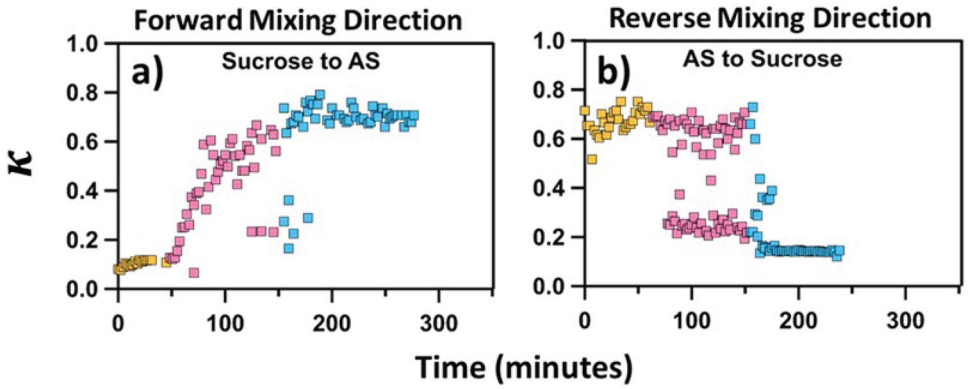

Figure 6. Experimental κ-values as retrieved by PyCat as a function of time for the forward (a) and reverse (b) mixing directions.

(approximately 0.4 difference in κ) to be effectively identified as distinct sigmoid curves. The finding in regard to the particle-to-particle heterogeneity of mixtures has recently been supported by the work of Yuan and Zhao 2023; who used HTDMA data sets. While their work focuses on field observations, they also stress the importance of capturing the kappa-distribution of an aerosol and the fact that the mean kappa value of a population can be very misleading in characterizing its hygroscopicity.

The evolution of κ-values over time is shown in Figure 6. In both the forward and reverse mixing directions, experimental results confirm that, during phase one and phase three, only one species with a single κ-value of either $\kappa_{\text{ammonium sulfate}}$ or κ_{sucrose} is present in the system, which agreed with the simulations. During phase 2, κ-values retrieved by PyCat for the forward mixing experiment showed a single κ-value that gradually increases with time and ammonium sulfate content in the mixing tube. This occurs because not enough time has elapsed for aerosol particles to traverse the tube. It is also indicative of a complex transient state where experimental results are difficult to interpret. At the end of phase 2, PyCat was able to identify two distinct κ-values. In comparison, PyCat consistently identified two distinct κ-values in the reverse direction. In both cases, experimental data and subsequent analysis were unable to capture the κ distribution simulated by PartMC. As such, information on the effects of aerosol mixing states on measured particle water-uptake from the experimentally derived κ may be incomplete and not representative of the system.

Summary and implications

The current size-resolved CCN analysis software (PyCAT) can rapidly provide activation curves of populations that are either internally mixed or fully externally mixed (subpopulations exist that can differ in their κ values, but within each subpopulation all particles have the same κ). CCN analysis using PyCAT results in the highest resolution data, with over tenfold more data points over each two-minute scan compared to experiments operated at a constant diameter for a range of supersaturations. However, for complex mixtures that are neither fully internal nor externally mixed, the experimentalist is still responsible for determining how many sigmoid curves would be sufficient to capture the mixing state of a system during one activation scan. In this work, we used a model system of ammonium sulfate and sucrose to demonstrate the usage and integration of a particle mixing model to assist in activation determination of size resolved CCN analysis.

For single component systems, PartMC simulated the experimental observations with very good agreement. In comparison, for more complex binary mixtures, PartMC predicted that the presence of particles consisting of two pure compounds dominated the system at diameters that activate at 0.86% supersaturation, and that some mixed particles were also present at much lower number concentrations. Knowledge of the relative abundance of the mixed particles and their predicted activation curves is valuable information for fitting sigmoid curves onto experimental data. In this case, although mixed particles are predicted to be present, their low number concentrations suggest that their contribution to the hygroscopicity of the system is minimal. As such, experimental data can be sufficiently fit with two sigmoid curves, one for each pure compound. The model predicts that given the initial size distributions, mixed particles are more prevalent at larger diameters (corresponding to activation at lower supersaturations) and recreating the mixing evolution at such conditions is a suggested future direction. This work confirms that the integration of a particle mixing model to further improve the size resolved CCN analysis method leads to more insight into the mixing evolution of aerosol particles. This improvement in analysis is valuable, especially when working with complex or unknown systems such as ambient aerosols.

Author contribution

AAA, PNR, and KAM designed and conducted the mixing tube water-uptake experiments. KG performed the PyCat Data analysis. NR and AD conducted the Part MC simulations. PNR conducted analysis across the datasets and prepared the manuscript with input from all coauthors.

Disclosure statement

The authors declare that they have no conflict of interest.

Funding

PNR, KAM, KG, and AAA acknowledge support from the National Science Foundation: AGS-1723920 and AGS-2124489. NR acknowledges support from AGS-1941110.

ORCID

Patricia N. Razafindrambinina http://orcid.org/0000-0002-1553-5839
Nicole Riemer http://orcid.org/0000-0002-3220-3457
Akua A. Asa-Awuku http://orcid.org/0000-0002-0354-8368

Data availability

The data is available upon request from the corresponding author as stated.

References

Andreae, M. O., and D. Rosenfeld. 2008. Aerosol–cloud–precipitation interactions. Part 1. The nature and sources of cloud-active aerosols. *Earth. Sci. Rev.* 89 (1–2):13–41. doi:10.1016/j.earscirev.2008.03.001.

Aneja, V. P., J. Blunden, K. James, W. H. Schlesinger, R. Knighton, W. Gilliam, G. Jennings, D. Niyogi, and S. Cole. 2008. Ammonia Assessment from Agriculture: U.S. Status and Needs. *J. Environ. Qual.* 37 (2):515–20. doi:10.2134/jeq2007.0002in.

Behera, S. N., M. Sharma, V. P. Aneja, and R. Balasubramanian. 2013. Ammonia in the atmosphere: A review on emission sources, atmospheric chemistry and deposition on terrestrial bodies. *Environ. Sci. Pollut. Res. Int.* 20 (11):8092–131. doi:10.1007/s11356-013-2051-9.

Bondy, A. L., D. Bonanno, R. C. Moffet, B. Wang, A. Laskin, and A. P. Ault. 2018. The diverse chemical mixing state of aerosol particles in the southeastern United States. *Atmos. Chem. Phys.* 18 (16):12595–612. doi:10.5194/acp-18-12595-2018.

Cruz, C. N., and S. N. Pandis. 1998. The effect of organic coatings on the cloud condensation nuclei activation of inorganic atmospheric aerosol. *J. Geophys. Res.* 103 (D11):13111–23. doi:10.1029/98JD00979.

Cubison, M. J., B. Ervens, G. Feingold, K. S. Docherty, I. M. Ulbrich, L. Shields, K. Prather, S. Hering, and J. L. Jimenez. 2008. The influence of chemical composition and mixing state of Los Angeles urban aerosol on CCN number and cloud properties. *Atmos. Chem. Phys.* 8 (18):5649–67. doi:10.5194/acp-8-5649-2008.

Curtis, J. H., M. D. Michelotti, N. Riemer, M. T. Heath, and M. West. 2016. Accelerated simulation of stochastic particle removal processes in particle-resolved aerosol models. *Comput. Phys.* 322:21–32. doi:10.1016/j.jcp.2016.06.029.

Dawson, J. N., K. A. Malek, P. N. Razafindrambinina, T. M. Raymond, D. D. Dutcher, A. A. Asa-Awuku, and M. A. Freedman. 2020. Direct comparison of the submicron aerosol hygroscopicity of water-soluble sugars. *ACS Earth Space Chem.* 4 (12):2215–26. doi:10.1021/acsearthspacechem.0c00159.

DeVille, N., M. Riemer, and West, L. 2019. Convergence of a generalized weighted flow algorithm for stochastic particle coagulation. *J. Comput. Dyn.* 6 (1):69–94. doi:10.3934/jcd.2019003.

DeVille, R. E. L., N. Riemer, and M. West. 2011. Weighted Flow Algorithms (WFA) for stochastic particle coagulation. *Comput. Phys.* 230 (23):8427–51. doi:10.1016/j.jcp.2011.07.027.

Dusek, U., G. P. Frank, L. Hildebrandt, J. Curtius, J. Schneider, S. Walter, D. Chand, F. Drewnick, S. Hings, D. Jung, et al. 2006. Size matters more than chemistry aerosol particles. *Science* 312 (5778):1375–8. doi:10.1126/science.1125261.

Feingold, G. 2003. Modeling of the first indirect effect: Analysis of measurement requirements. *Geophys. Res. Lett.* 30 (19):1–4. doi:10.1029/2003GL017967.

Fofie, E. A., N. M. Donahue, and A. Asa-Awuku. 2018. Cloud condensation nuclei activity and droplet formation of primary and secondary organic aerosol mixtures. *Aerosol Sci. Technol.* 52 (2):242–51. doi:10.1080/02786826.2017.1392480.

Gohil, K., and A. A. Asa-Awuku. 2022. Cloud condensation nuclei (CCN) activity analysis of low-hygroscopicity aerosols using the aerodynamic aerosol classifier (AAC). *Atmos. Meas. Tech.* 15 (4):1007–19. doi:10.5194/amt-15-1007-2022.

Hudson, J. G. 2007. Variability of the relationship between particle size and cloud-nucleating ability. *Geophys. Res. Lett.* 34:1–5. doi:10.1029/2006GL028850.

Kim, N., S. S. Yum, M. Park, J. S. Park, H. J. Shin, and J. Y. Ahn. 2020. Hygroscopicity of urban aerosols and its link to size-resolved chemical composition during spring and summer in Seoul, Korea. *Atmos. Chem. Phys.* 20 (19):11245–62. doi:10.5194/acp-20-11245-2020.

Kreidenweis, S. M., and A. Asa-Awuku. 2014. Aerosol hygroscopicity: Particle water content and its role in atmospheric processes. In *Treatise on Geochemistry*, eds. Heinrich D. Holland and Karl K. Turekian, 2nd ed., 331–361. Elsevier. doi:10.1016/B978-0-08-095975-7.00418-6.

Lambe, A. T., T. B. Onasch, P. Massoli, D. R. Croasdale, J. P. Wright, A. T. Ahern, L. R. Williams, D. R. Worsnop, W. H. Brune, and P. Davidovits. 2011. Laboratory studies of the chemical composition and cloud condensation nuclei (CCN) activity of secondary organic aerosol (SOA) and oxidized primary organic aerosol (OPOA). *Atmos. Chem. Phys.* 11 (17):8913–28. doi:10.5194/acp-11-8913-2011.

Lance, S., T. Raatikainen, T. B. Onasch, D. R. Worsnop, X. Y. Yu, M. L. Alexander, M. R. Stolzenburg, P. H. McMurry, J. N. Smith, and A. Nenes. 2013. Aerosol mixing state, hygroscopic growth and cloud activation

efficiency during MIRAGE 2006. *Atmos. Chem. Phys.* 13 (9):5049–62. doi:10.5194/acp-13-5049-2013.

Lei, T., A. Zuend, W. G. Wang, Y. H. Zhang, and M. F. Ge. 2014. Hygroscopicity of organic compounds from biomass burning and their influence on the water uptake of mixed organic ammonium sulfate aerosols. *Atmos. Chem. Phys.* 14 (20):11165–83. doi:10.5194/acp-14-11165-2014.

Marynowski, L., and B. R. T. Simoneit. 2022. Saccharides in atmospheric particulate and sedimentary organic matter: Status overview and future perspectives. *Chemosphere* 288 (Pt 1):132376. doi:10.1016/j.chemosphere.2021.132376.

Moore, R. H., and A. Nenes. 2009. Scanning flow CCN analysis method for fast measurements of CCN spectra. *Aerosol Sci. Technol.* 43 (12):1192–207. doi:10.1080/02786820903289780.

Moore, R. H., A. Nenes, and J. Medina. 2010. Scanning mobility CCN analysis-A method for fast measurements of size-resolved CCN distributions and activation kinetics. *Aerosol Sci. Technol.* 44 (10):861–71. doi:10.1080/02786826.2010.498715.

Peng, C., P. N. Razafindrambinina, K. A. Malek, L. Chen, W. Wang, R.-J. Huang, Y. Zhang, X. Ding, M. Ge, X. Wang, et al. 2021. Interactions of organosulfates with water vapor under sub- and supersaturated conditions. *Atmos. Chem. Phys.* 21 (9):7135–48. doi:10.5194/acp-21-7135-2021.

Petters, M. D., and S. M. Kreidenweis. 2007. A single parameter representation of hygroscopic growth and cloud condensation nucleus activity. *Atmos. Chem. Phys.* 7 (8):1961–71. doi:10.5194/acp-7-1961-2007.

Petters, M. D., and S. M. Kreidenweis. 2008. A single parameter representation of hygroscopic growth and cloud condensation nucleus activity - Part 2: Including solubility. *Atmos. Chem. Phys.* 8 (20):6273–9. doi:10.5194/acp-8-6273-2008.

Petters, M. D., and S. M. Kreidenweis. 2013. A single parameter representation of hygroscopic growth and cloud condensation nucleus activity-Part 3: Including surfactant partitioning. *Atmos. Chem. Phys.* 13 (2):1081–91. doi:10.5194/acp-13-1081-2013.

Razafindrambinina, P. N., K. A. Malek, J. N. Dawson, K. DiMonte, T. M. Raymond, D. D. Dutcher, M. A. Freedman, and A. Asa-Awuku. 2022. Hygroscopicity of internally mixed ammonium sulfate and secondary organic aerosol particles formed at low and high relative humidity. *Environ. Sci.: Atmos.* 2 (2):202–14. doi:10.1039/D1EA00069A.

Riemer, N., A. P. Ault, M. West, R. L. Craig, and J. H. Curtis. 2019. Aerosol mixing state: Measurements, modeling, and impacts. *Rev. Geophys.* 57 (2):187–249. doi:10.1029/2018RG000615.

Riemer, N., M. West, R. A. Zaveri, and R. C. Easter. 2009. Simulating the evolution of soot mixing state with a particle-resolved aerosol model. *J. Geophys. Res.* 114 (D9):1–22. doi:10.1029/2008JD011073.

Roberts, G. C., P. Artaxo, J. Zhou, E. Swietlicki, and M. O. Andreae. 2002. Sensitivity of CCN spectra on chemical and physical properties of aerosol : A case study from the Amazon Basin. *J. Geophys. Res.: Atmos.* 107:1–18. doi:10.1029/2001JD000583.

Shou, C., N. Riemer, T. B. Onasch, A. J. Sedlacek, A. T. Lambe, E. R. Lewis, P. Davidovits, and M. West. 2019. Mixing state evolution of agglomerating particles in an aerosol chamber: Comparison of measurements and particle-resolved simulations. *Aerosol Sci. Technol.* 53 (11):1229–43. doi:10.1080/02786826.2019.1661959.

Stokes, R. H., and R. A. Robinson. 1966. Interactions in aqueous nonelectrolyte solutions. I. Solute-solvent equilibria. *J. Phys. Chem.* 70 (7):2126–31. doi:10.1021/j100879a010.

Svenningsson, B., J. Rissler, E. Swietlicki, M. Mircea, M. Bilde, M. C. Facchini, S. Decesari, S. Fuzzi, J. Zhou, J. Mønster, et al. 2006. Hygroscopic growth and critical supersaturations for mixed aerosol particles of inorganic and organic compounds of atmospheric relevance. *Atmos. Chem. Phys.* 6 (7):1937–52. doi:10.5194/acp-6-1937-2006.

Tian, J., B. T. Brem, M. West, T. C. Bond, M. J. Rood, and N. Riemer. 2017. Simulating aerosol chamber experiments with the particle-resolved aerosol model PartMC. *Aerosol Sci. Technol.* 51 (7):856–67. doi:10.1080/02786826.2017.1311988.

Tian, J., N. Riemer, M. West, L. Pfaffenberger, H. Schlager, and A. Petzold. 2014. Modeling the evolution of aerosol particles in a ship plume using PartMC-MOSAIC. *Atmos. Chem. Phys.* 14 (11):5327–47. doi:10.5194/acp-14-5327-2014.

Vu, D., S. Gao, T. Berte, M. Kacarab, Q. Yao, K. Vafai, and A. Asa-Awuku. 2019. External and internal cloud condensation nuclei (CCN) mixtures: Controlled laboratory studies of varying mixing states. *Atmos. Meas. Tech.* 12 (8):4277–89. doi:10.5194/amt-12-4277-2019.

Wang, Q., L. Li, J. Zhou, J. Ye, W. Dai, H. Liu, Y. Zhang, R. Zhang, J. Tian, Y. Chen, et al. 2020. Measurement report: Source and mixing state of black carbon aerosol in the North China Plain: Implications for radiative effect. *Atmos. Chem. Phys.* 20 (23):15427–42. doi:10.5194/acp-20-15427-2020.

Winkler, P. 1973. The growth of atmospheric aerosol particles as a function of the relative humidity—II. An improved concept of mixed nuclei. *J. Aerosol Sci.* 4 (5):373–87. doi:10.1016/0021-8502(73)90027-X.

Xu, W., J. Ovadnevaite, K. N. Fossum, C. Lin, R.-J. Huang, C. O'Dowd, and D. Ceburnis. 2020. Aerosol hygroscopicity and its link to chemical composition in the coastal atmosphere of Mace Head: Marine and continental air masses. *Atmos. Chem. Phys.* 20 (6):3777–91. doi:10.5194/acp-20-3777-2020.

Ye, Q., E. S. Robinson, X. Ding, P. Ye, R. Sullivan, and N. Robinson. 2016. Mixing of secondary organic aerosols versus relative humidity. *Proc. Natl. Acad. Sci. U S A* 113 (45):12649–54. doi:10.1073/pnas.1604536113.

Yuan, L., and C. Zhao. 2023. Quantifying particle-to-particle heterogeneity in aerosol hygroscopicity. *Atmos. Chem. Phys.* 23 (5):3195–205. doi:10.5194/acp-23-3195-2023.

Zaveri, R. A., J. C. Barnard, R. C. Easter, N. Riemer, and M. West. 2010. Particle-resolved simulation of aerosol size, composition, mixing state, and the associated optical and cloud condensation nuclei activation properties in an evolving urban plume. *J. Geophys. Res.* 115 (D17):D17210. doi:10.1029/2009JD013616.

Zhao, D. F., A. Buchholz, B. Kortner, P. Schlag, F. Rubach, A. Kiendler-Scharr, R. Tillmann, A. Wahner, J. M. Flores, Y. Rudich, et al. 2015. Size-dependent hygroscopicity parameter (κ) and chemical composition of secondary organic cloud condensation nuclei. *Geophys. Res. Lett.* 42 (24):10–,920. doi:10.1002/2015GL066497.